
Empowering Source-Free Domain Adaptation with MLLM-driven Curriculum Learning

Dongjie Chen¹ Kartik Patwari¹ Zhengfeng Lai¹ Sen-ching Cheung^{1,2} Chen-Nee Chuah¹

¹ University of California, Davis ² University of Kentucky

{cdjchen, kpatwari, lzhengfeng, chuah}@ucdavis.edu, sccheung@ieee.org

Abstract

Source-Free Domain Adaptation (SFDA) aims to adapt a pre-trained source model to a target domain using only unlabeled target data. Current SFDA methods face challenges in effectively leveraging pre-trained knowledge and exploiting target domain data. Multimodal Large Language Models (MLLMs) offer remarkable capabilities in understanding visual and textual information, but their applicability to SFDA poses challenges such as instruction-following failures, intensive computational demands, and difficulties in performance measurement prior to adaptation. To alleviate these issues, we propose Reliability-based Curriculum Learning (RCL), a novel framework that integrates multiple MLLMs for knowledge exploitation via pseudo-labeling in SFDA. Our framework incorporates proposed Reliable Knowledge Transfer, Self-correcting and MLLM-guided Knowledge Expansion, and Multi-hot Masking Refinement to progressively exploit unlabeled data in the target domain. RCL achieves state-of-the-art (SOTA) performance on multiple SFDA benchmarks, e.g., **+9.4%** on DomainNet, demonstrating its effectiveness in enhancing adaptability and robustness without requiring access to source data. Code: <https://github.com/Dong-Jie-Chen/RCL>

1 Introduction

Although Unsupervised Domain Adaptation (UDA) holds promise for addressing domain shift by leveraging labeled data from a source domain, its effectiveness heavily relies on a well-curated labeled source dataset, which is time-consuming and labor-intensive to build [1, 2, 3]. Moreover, practical constraints such as data privacy concerns, storage limitations often hinder access to such labeled sources. In response, Source-Free Domain Adaptation (SFDA) has gained attention as a more practical solution [4]. SFDA aims to transfer a pre-trained source model to a target domain using only unlabeled target data without access to the labeled source data.

One of the key aspects that make SFDA effective is the use of externally pre-trained models. Earlier works utilized models pre-trained on ImageNet [4], while more recent works shift towards using large-scale pre-trained models like CLIP [1, 2, 3, 5]. These pre-trained models have learned rich and transferable feature representations from vast amounts of labeled data, which can serve as a strong foundation to bridge the domain gap. However, the importance of pre-trained knowledge has been less explored in previous works [4]. As shown in Figure 1a, we observe that the zero-shot performance of pre-trained multimodal large language models (MLLMs), such as LLaVA [6] and InstructBLIP [7], outperform models pre-trained on ImageNet [8] or distilling knowledge from CLIP [5]. The advanced architectures and training techniques employed by these MLLMs have set new benchmarks in tasks like visual question answering (VQA), detailed description, and complex reasoning retrieval [6, 9, 10]. Remarkably, these MLLMs achieve superior results without having seen any images from either the source or target domain. Based on this observation, we hypothesize

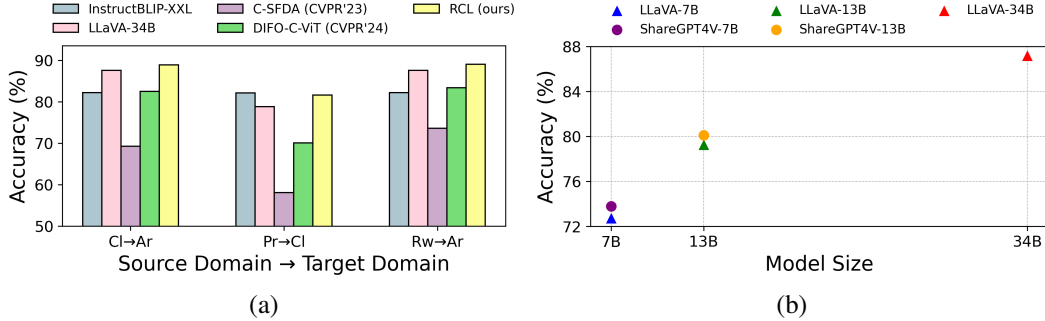


Figure 1: (a) Zero-shot performance comparison between MLLMs and recent methods on Office-Home, which consists of four domains. MLLMs demonstrate superior zero-shot performance compared to models pre-trained on ImageNet or distilling knowledge from CLIP; (b) Zero-shot ability of MLLMs with different model sizes on Office-Home. Larger models achieve higher accuracy but at the cost of increased computational demands.

that pre-trained models and pre-trained knowledge are important to improve the performances of SFDA. However, efforts to leverage them in domain adaptation tasks remain limited.

MLLMs have shown good performance in understanding visual and textual information [6, 7, 10, 11], but their applicability to SFDA classification tasks faces several challenges. First, as shown in Figure 3, MLLMs often struggle to follow instructions for zero-shot classification since they are primarily designed for text generation. Second, even though MLLMs have shown promising zero-shot ability, their inference process is time-consuming and computationally intensive, which prevents their wide adoption. Third, the performance of MLLMs varies significantly depending on their model size. As shown in Figure 1b, with smaller models like the 7B model yields suboptimal results and larger models like the 34B model achieving impressive performance at higher computational cost. For instance, inference with LLaVA-1.5-13B requires 155B FLOPS, which is 55% more than the 7B version of LLaVA-1.5 [12]. Additionally, domain-specific fine-tuning of MLLMs necessitates significant computational investment and a GPT-4-driven instruction-following dataset [7, 10], which pose scalability challenges across diverse downstream tasks. This highlights the need for efficient methods that leverage foundational MLLM knowledge in a way that maintains scalability for domain-specific adaptations.

To address these challenges, we propose a novel framework called Reliability-based Curriculum Learning (RCL, as shown in Figure 2), that enables an effective integration of multiple MLLMs with pseudo-labeling. We aim to distill the pre-trained knowledge to a small model, which allows us to avoid fine-tuning MLLMs and conduct large-scale inference after training for diverse tasks [4, 13]. Unlike existing works that rely solely on a single source of external information [2, 4, 5], our method leverages multiple MLLMs to achieve more robust adaptation in the following manners: First, we propose MLLM-driven pseudo-labeling to convert the VQA tasks into classification tasks to improve the zero-shot performance. Second, we improve the stability of the distillation process by recasting it as a curriculum learning problem using a consensus-based reliability measurement on pseudo-labels. In this CL process, we start learning from samples with the most reliable pseudo-labels, then gradually progress to less reliable ones. Lastly, traditional pseudo-labeling methods fail to exploit the entire dataset as they only retain the high-confident samples [5]. To address this issue, we propose a Multi-hot Masking technique that helps the model exploit samples that are not selected for pseudo-labeling. Not only can this approach fully leverage the entire unlabeled set, but it also helps the model learn from the varying predictions on the same samples from different MLLMs. Specifically, RCL achieves a **+6.7%** increase on Office-Home [13], **+9.4%** on DomainNet [14], and **+2.8%** on VisDA-C [15]. To summarize, our main contributions are:

- We utilize multiple MLLMs to perform zero-shot image classification and propose a consensus-based reliability measurement to assess the reliability of pseudo-labels obtained from multiple MLLMs.
- We introduce a Reliability-based Curriculum Learning (RCL) framework that proposes Reliable Knowledge Transfer (RKT), Self-correcting and MLLM-guided Knowledge Expansion

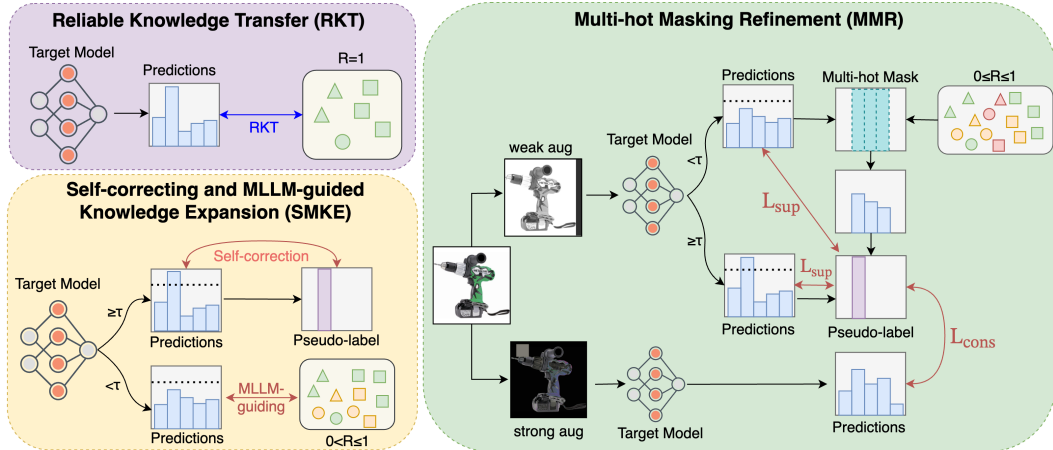


Figure 2: An overview of our proposed Reliability-based Curriculum Learning (RCL) framework.

(SMKE), and Multi-hot Masking Refinement (MMR) techniques to progressively distill the knowledge from MLLMs on the target domain data.

- Our approach achieves state-of-the-art results on multiple benchmarks, demonstrating its effectiveness in enhancing the adaptability and robustness of SFDA.

2 Related Work

Source-Free Domain Adaptation. Recent SFDA methods have explored various novel methodologies to adapt source-domain models but without the source data to a target domain. These methodologies include using unlabeled target data through neighborhood clustering techniques [16, 17], exploiting target data manifolds [18], and employing pseudo-labels [19, 20, 21]. Notably, SHOT [4] utilizes pseudo-labeling, freezing the source classifier, clustering target features, and maximizing mutual information. In addition to target data-based methods, there are other approaches focusing on aligning source and target data distributions [22] and minimizing the contrastive adaptation loss between feature distributions by leveraging semantic statistics of target data [23].

Vision-Language Models and Multimodal Large Language Models. Prominent VLMs like CLIP [24] and ALIGN [25] excel in capturing modality-invariant features to support diverse applications. The integration of Large Language Models (LLMs) and VLMs has spurred the development of MLLMs like GPT4-Vision. Notable examples include LLaVA [6, 10], which uses GPT-4 generated data for multimodal instruction tuning, enhancing general-purpose visual and language understanding; InstructBLIP [7] leverages a pre-trained BLIP-2 model and an instruction-aware Query Transformer; and ShareGPT4V [11] uses highly descriptive image captions from GPT4-Vision for better vision-language alignment. Recent trends [26, 27, 28] leverage VLMs to improve domain adaptation. For example, DAPL [1] utilizes prompt-based learning to bridge domain gaps. PADCLIP [2] combines frozen and finetuned CLIP vision encoder to debias zero-shot predictions and prevents catastrophic forgetting. A common limitation of these method is that they require significant amount of labeled source data. Recently, DIFO [5] achieves source-free domain adaptation by customizing CLIP for task-specific knowledge distillation via unsupervised prompt learning and predictive consistency. Unlike previous methods that depend on CLIP, our approach utilizes the zero-shot capabilities of various MLLMs for pseudo-labeling without any adaptation of large foundation models. We employ a curriculum learning strategy that trains the target model based on pseudo-label reliability and incorporates a self-iterative refinement process to improving adaptation effectiveness.

3 Methodology

Denote $\mathcal{D}_s = (x_s^i, y_s^i)_{i=1}^{N_s}$ as a labeled source domain dataset, where $x_s^i \in \mathcal{X}_s$ refers to an image and $y_s^i \in \mathcal{Y}_s$ is its corresponding label. The source domain data consist of N_s labeled images. A

pre-trained source model $f_{\theta_s} : \mathcal{X}_s \rightarrow \mathcal{Y}_s$ has been trained on the source domain dataset \mathcal{D}_s , where θ_s denotes the learned parameters of the source model. In the target domain, we have access to an unlabeled dataset $\mathcal{D}_t = \{x_t^i\}_{i=1}^{N_t}$, where $x_t^i \in \mathcal{X}_t$ is an image from the target domain, and N_t is the number of unlabeled images. The goal of source-free domain adaptation is to adapt the pre-trained source model f_{θ_s} to the target domain \mathcal{D}_t without access to the source data \mathcal{D}_s during the adaptation process. The objective is to train a target model $f_{\theta_t} : \mathcal{X}_t \rightarrow \mathcal{Y}_t$ on the target domain, where \mathcal{Y}_t represents the label space in the target domain.

3.1 Pseudo-labeling with MLLMs

We focus on exploiting multiple MLLMs to provide the initial mappings between the target images to the unlabeled target domain. As MLLMs are primarily designed for text generation tasks, they may not be directly applicable to image classification tasks. We formulate a prompt engineering solution to enable MLLMs to predict class labels only. Figure 3 shows our approach about converting a visual question answering (VQA) task into a zero-shot multi-class classification problem. We construct the prompt input by concatenating a list of options, representing all class names in the dataset, with a question asking the MLLMs to select the most appropriate class from the given options. We then feed the prompt and image x_t^i to multiple pre-trained MLLMs, such as LLaVA [6, 10], InstructBLIP [7], and ShareGPT4V [11], which process the prompt and generate their respective text outputs $T_1^i, T_2^i, \dots, T_M^i$, where M is the number of MLLMs employed.

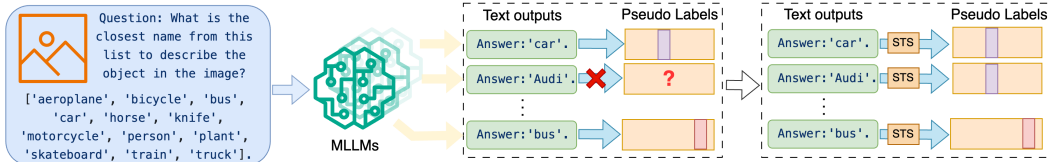


Figure 3: Pseudo-labeling with MLLMs. Directly prompting MLLMs for classification can lead to failures: we propose semantic textual similarity (STS) (in Section 3.1).

However, as shown in Figure 3, MLLMs sometimes fail to follow the instructions in the input prompt. Based on our observations, this usually happens when MLLMs can still understand the content of the image while providing a text description based on their own knowledge instead of picking the closest answer from the list (e.g., generating ‘Audi’ when the groundtruth label is ‘car’). To address this issue and ensure that the pseudo-labels accurately reflect the intended class names, we propose using semantic textual similarity (STS) to measure the similarity between the generated text outputs and the provided text options.

To obtain pseudo-labels from the generated text outputs, we measure the STS between the text options and each MLLM’s output. Formally, for the m -th MLLM and the i -th image x_t^i , the pseudo-label \hat{y}^{mi} is determined by:

$$\hat{y}^{mi} = \underset{c}{\operatorname{argmin}} \operatorname{STS}(T_m^i, T_t^c), \quad (1)$$

where T_t^c represents the text option for the c -th class. The STS between two text sequences T_1 and T_2 is computed as:

$$\operatorname{STS}(T_1, T_2) = 1 - \frac{\mathbf{v}_1 \cdot \mathbf{v}_2}{\|\mathbf{v}_1\|_2 \|\mathbf{v}_2\|_2}, \quad (2)$$

where \mathbf{v}_1 and \mathbf{v}_2 are vector representations of T_1 and T_2 , respectively. By assigning the pseudo-labels \hat{y}^{mi} that minimize the STS between the generated text output and the text options for each sample x_t^i , we ensure that the pseudo-labels accurately reflect the most semantically similar class names, even when the MLLMs fail to strictly adhere to the provided instructions (implementation details are provided in Section 4.3).

3.2 Consensus-Based Reliability Measurement

The pseudo-labels generated by multiple MLLMs for each target domain sample may not always reach a consensus. This disagreement among the MLLMs raises a crucial question: **how can we measure the reliability of the pseudo-labels from multiple MLLMs?** STS is not suitable for assessing the reliability of the pseudo-labels because it cannot determine if the MLLMs are predicting

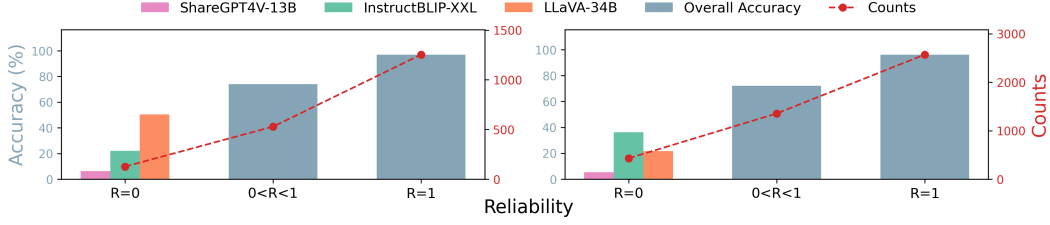


Figure 4: Accuracy and distribution of pseudo-labels using LLaVA, InstructBLIP and ShareGPT4V. Left: Office-Home Clipart domain, Right: Office-Home Art domain. Both domains have 65 classes.

the wrong label, as its primary focus is on correcting the MLLMs’ behavior when they fail to follow the instructions. Consequently, we need to design a separate method for reliability measurement. To address this challenge, we introduce a consensus-based reliability measuring strategy.

We define a reliability measure $\mathcal{R}(x_t^i)$ for each target domain sample x_t^i based on the agreement among the pseudo-labels assigned by different MLLMs:

$$\mathcal{R}(x_t^i) = \frac{1}{M(M-1)} \sum_{m=1}^M \sum_{n=1, n \neq m}^M \mathbb{1}(\hat{y}^{mi} = \hat{y}^{ni}), \quad (3)$$

where $\mathbb{1}(\cdot)$ is the indicator function. The reliability measure $\mathcal{R}(x_t^i)$ represents the proportion of MLLM pairs that agree on the pseudo-label for the sample x_t^i . Based on the reliability measure, we divide the target dataset \mathcal{D}_t into three subsets: $\mathcal{D}_t = \{\mathcal{D}_R, \mathcal{D}_{LR}, \mathcal{D}_{UR}\}$, where \mathcal{D}_R , \mathcal{D}_{LR} , and \mathcal{D}_{UR} represent the reliable (all MLLMs agree, $\mathcal{R}(x_t^i) = 1$), less reliable (between all agree and all disagree, $0 < \mathcal{R}(x_t^i) < 1$), and unreliable (all MLLMs disagree, $\mathcal{R}(x_t^i) = 0$) subsets, respectively. As shown in Figure 4, samples with higher reliability scores tend to have higher pseudo-label accuracy, validating the effectiveness of our consensus-based reliability measurement strategy. Figure 4 shows the accuracy and distribution of pseudo-labels with different reliability ($\mathcal{R}(x_t^i)$) that reflects the level of disagreements among LLaVA, InstructBLIP, and ShareGPT4V. When $\mathcal{R}(x_t^i) = 0$, we show the accuracy of individual MLLM.

3.3 Reliability-based Curriculum Learning framework

Building upon the consensus-based reliability measure and the categorization of the target dataset, we propose a Reliability-based Curriculum Learning framework (RCL) to strategically leverage target domain data. As shown in Figure 2, the RCL process unfolds as follows:

1. In Section 3.3.1, we begin by training the target model solely on the reliable subset \mathcal{D}_R .
2. In Section 3.3.2, we progress to fine-tuning the target model using both the reliable and less reliable subsets $\mathcal{D}_R \cup \mathcal{D}_{LR}$, applying a confidence-based pseudo-label selection strategy.
3. In Section 3.3.3, we conclude by fine-tuning the target model using the entire target domain dataset \mathcal{D}_t , incorporating the Multi-hot Masking approach and consistency regularization for the unreliable subset \mathcal{D}_{UR} .

This approach ensures that the model initially learns from the most reliable samples, building a strong foundational knowledge. This foundation is progressively refined by incorporating less reliable data, thus regularizing the learning trajectory and avoiding potential pitfalls of starting training with all data simultaneously.

3.3.1 Reliable Knowledge Transfer

First, we focus on transferring the most reliable knowledge from the MLLMs to the target model. Reliable Knowledge Transfer (RKT) uses the pseudo-labels of the samples in the reliable subset \mathcal{D}_R to train the target model in a supervised manner. Since the model has not yet learned any information from the target data at this stage, we fully rely on the most reliable knowledge provided by the MLLMs to train the target model. The reliable subset \mathcal{D}_R consists of samples for which all MLLMs agree on the pseudo-label:

$$\mathcal{D}_R = \{(x_r^i, y_r^i) \mid \mathcal{R}(x_r^i) = 1\}, \quad (4)$$

where x_r^i is the i -th sample in the reliable subset, y_r^i is the corresponding pseudo-label agreed upon by all MLLMs, and $\mathcal{R}(x_r^i)$ is the reliability measure defined in the previous section. The target model f_{θ_t} is trained using a supervised cross-entropy loss on the reliable subset \mathcal{D}_R :

$$\mathcal{L}_{RKT} = -\frac{1}{|\mathcal{D}_R|} \sum_{(x_r^i, y_r^i) \in \mathcal{D}_R} y_r^i \cdot \log f_{\theta_t}(x_r^i), \quad (5)$$

where $|\mathcal{D}_R|$ denotes the number of samples in the reliable subset. By training the target model on the reliable subset \mathcal{D}_R , we aim to transfer the most confident and consistent knowledge from the MLLMs to the target model. RKT helps the target model to establish a strong foundation based on the reliable pseudo-labels before proceeding to the less reliable knowledge.

3.3.2 Self-correcting and MLLM-guided Knowledge Expansion

After RKT, the RCL process expands to include samples with less reliable pseudo-labels. Given that the target model has been pre-trained on the source model and fine-tuned with RKT, we can now leverage the target model’s own predictions for self-correction when the model is confident, and utilize the MLLMs to guide the target model when it is less confident. To achieve this, we introduce Self-correcting and MLLM-guided Knowledge Expansion (SMKE).

To incorporate the less reliable pseudo-labels, we fine-tune the target model using samples from both the reliable and less reliable subsets $\mathcal{D}_R \cup \mathcal{D}_{LR}$. This enables the target model to learn from a larger portion of the target domain data and benefit from the additional information provided by \mathcal{D}_{LR} .

In SMKE, the pseudo-label \tilde{y}^i used for training the target model is determined based on the confidence of the target model’s predictions. Let \hat{y}_t^i be the pseudo-label predicted by the target model for the target domain sample x_t^i , and let p_t^i be the corresponding confidence score, which is calculated as the maximum value of the target model’s predictive probabilities. We define a confidence threshold τ to determine whether to use the target model’s pseudo-label or the MLLMs’ pseudo-label. The pseudo-label \tilde{y}^i is as follows:

$$\tilde{y}^i = \begin{cases} \hat{y}_t^i, & \text{if } p_t^i \geq \tau \\ \text{mode}(y^{1i}, y^{2i}, \dots, y^{Mi}), & \text{if } p_t^i < \tau \end{cases} \quad (6)$$

where $\text{mode}(\cdot)$ returns the most frequent pseudo-label among the MLLMs.

In SMKE, if the target model’s confidence score p_t^i is greater than or equal to the threshold τ , we employ the target model’s pseudo-label \hat{y}_t^i for self-correction. Conversely, if the target model’s confidence score falls below the threshold, indicating insufficient knowledge of the given samples, we resort to the most frequent pseudo-label among the MLLMs for knowledge expansion. The adaptive training approach is optimized through the loss function:

$$\mathcal{L}_{SMKE} = -\frac{1}{|\mathcal{D}_R \cup \mathcal{D}_{LR}|} \sum_{x_t^i \in \{\mathcal{D}_R \cup \mathcal{D}_{LR}\}} \tilde{y}^i \cdot \log f_{\theta_t}(x_t^i) \quad (7)$$

By incorporating the less reliable pseudo-labels and leveraging the target model’s confidence scores, the SMKE stage of the curriculum learning framework aims to expand the knowledge transferred to the target model by utilizing both the target model’s predictions and the MLLMs’ pseudo-labels.

3.3.3 Multi-hot Masking Refinement

Finally, we expand to the full training set to utilize the samples in the unreliable subset \mathcal{D}_{UR} , which consists of target domain samples where the MLLMs disagree on the pseudo-labels. The lack of consensus among the MLLMs makes it challenging to assign reliable pseudo-labels to the samples in \mathcal{D}_{UR} . As a result, these samples are not included in the training process during RKT and SMKE. To leverage the full spectrum of the target domain dataset \mathcal{D}_t , as shown in Figure 2, we propose Multi-hot Masking Refinement (MMR), which integrates joint selection and refinement mechanisms along with a consistency loss to effectively utilize these challenging samples.

Multi-hot Masking. Let $\mathbf{z}_t^i \in \mathbb{R}^C$ be the predictive probabilities of the target model for the target domain sample x_t^i , where C is the number of classes. The confidence score of the target model’s prediction is given by $p_t^i = \max_c \mathbf{z}_t^i$. We define a Multi-hot mask $\mathbf{m}^i \in \{0, 1\}^C$ based on the

pseudo-labels assigned by the MLLMs: $\mathbf{m}^i = 1 - \prod_{m=1}^M (1 - \mathbb{1}(\hat{y}^{mi}))$ where the mask \mathbf{m}^i is formed by adding up one-hot vectors indicating the presence of each class as predicted by the MLLMs for the sample x_t^i . We then apply the Multi-hot mask to mask out the target model’s logits, forming a refined pseudo-label \tilde{y}^i based on the confidence threshold τ :

$$\tilde{y}^i = \begin{cases} \operatorname{argmax}(\mathbf{z}_t^i), & \text{if } p_t^i \geq \tau \\ \operatorname{argmax}(\mathbf{z}_t^i \odot \mathbf{m}^i), & \text{if } p_t^i < \tau \end{cases} \quad (8)$$

where \odot denotes the element-wise multiplication, and τ is the confidence threshold. If p_t^i exceeds the threshold τ , the original prediction is retained. Otherwise, the prediction is adjusted to consider only those classes that are indicated by the multi-hot masking, effectively filtering out less likely class predictions.

$$\mathcal{L}_{\text{sup}} = -\frac{1}{|\mathcal{D}_R \cup \mathcal{D}_{LR} \cup \mathcal{D}_{UR}|} \sum_{x_t^i \in \{\mathcal{D}_R \cup \mathcal{D}_{LR} \cup \mathcal{D}_{UR}\}} \tilde{y}^i \cdot \log f_{\theta_t}(x_t^i) \quad (9)$$

The consistency loss $\mathcal{L}_{\text{cons}}$ is calculated using the refined pseudo-labels from both weak and strong augmented samples, reinforcing the target model’s predictions to align with those of the MLLMs, especially when the model is not confident:

$$\mathcal{L}_{\text{cons}} = \frac{1}{M} \sum_{m=1}^M \sum_{i=1}^{N_t} \mathbf{H}(\tilde{y}^i, \mathbf{z}_{st}^i) \quad (10)$$

where \mathbf{z}_{st}^i denotes the target model’s logit for strong augmentation samples and $\mathbf{H}(\cdot, \cdot)$ denotes the cross-entropy loss. The target model is then optimized through the combined loss $\mathcal{L}_{\text{MMR}} = \mathcal{L}_{\text{sup}} + \lambda_{\text{cons}} \mathcal{L}_{\text{cons}}$ where λ_{cons} is a fixed hyperparameter to balance the supervised and consistency losses. Through the MMR phase, the target model not only uses the MLLMs’ pseudo-labels to refine its training strategy but also ensures robust learning even from samples whose initial predictions lack confidence.

4 Experiments

4.1 Experimental Setup

Datasets. We evaluate our method on three standard benchmark datasets: Office-Home, DomainNet-126, and VisDA-C 2017. **Office-Home** [13] has 4 domains – Real (R), Clipart (C), Art (A), and Product (P), encompassing 65 classes with a total of 15.5k images. **VisDA** [15] is a large-scale synthetic-to-real object recognition dataset, where the source domain includes 152k synthetic images and the target domain contains about 55k real object images across 12 classes. **DomainNet** [14] is a challenging large-scale, featuring 6 domains with a total of around 600k images across 345 classes. We follow the standard DomainNet-126 setup with 145k images from 126 classes, sampled from four domains, Clipart (C), Painting (P), Real (R), Sketch (S).

Model details. Following prior work [5, 29, 30, 31], we utilize a ResNet-101 [32] backbone for VisDA and ResNet-50 for Office-Home and DomainNet. For VisDA and Office-Home, we employ pre-trained source models provided by SHOT [29]. For DomainNet, we train the source models from scratch, adopting the training regime and hyperparameters outlined in [33]. The parameters used in the training process of RCL are shown in Table 1. We use the Adam optimizer [34] for RCL training. All experiments are conducted using PyTorch on NVIDIA A100 GPUs. We utilize three open-source MLLMs (LLaVA-v1.6-34B [10], ShareGPT4V-13B [11], and InstructBLIP-Flan-T5-XXL [7]).

Table 1: Parameters for Different Datasets and Methods

	Office-Home			DomainNet			VisDA		
	RKT	SMKE	MMR	RKT	SMKE	MMR	RKT	SMKE	MMR
learning rate	1e-04	1e-05	1e-05	1e-05	1e-05	1e-05	1e-05	1e-06	1e-06
τ	–	0.7	0.95	–	0.7	0.9	–	0.7	0.6
batch size	64	256	128	64	256	64	64	256	256
max iter	3000	5000	5000	8000	10000	5000	6000	6000	5000

Table 2: Accuracy (%) on the **Office-Home**. SF denotes source-free, and CP, ViT denote the method using CLIP, and ViT backbone respectively. We highlight the best result and underline the second best one. (*) represents pre-trained CLIP/MLLM zero-shot performance.

Method	SF	CP	ViT	A→C	A→P	A→R	C→A	C→P	C→R	P→A	P→C	P→R	R→A	R→C	R→P	Avg.
Source	-	✗	✗	44.7	64.2	69.4	48.3	57.9	60.3	49.5	40.3	67.2	59.7	45.6	73.0	56.7
DAPL-RN [1]	✗	✓	✗	54.1	84.3	84.8	74.4	83.7	85.0	74.5	54.6	84.8	75.2	54.7	83.8	74.5
PADCLIP-RN [2]	✗	✓	✗	57.5	84.0	83.8	77.8	85.5	84.7	76.3	59.2	85.4	78.1	60.2	86.7	76.6
ADCLIP-RN [3]	✗	✓	✗	55.4	85.2	85.6	76.1	85.8	86.2	76.7	56.1	85.4	76.8	56.1	85.5	75.9
SHOT [29]	✓	✗	✗	56.7	77.9	80.6	68.0	78.0	79.4	67.9	54.5	82.3	74.2	58.6	84.5	71.9
NRC [35]	✓	✗	✗	57.7	80.3	82.0	68.1	79.8	78.6	65.3	56.4	83.0	71.0	58.6	85.6	72.2
GKD [36]	✓	✗	✗	56.5	78.2	81.8	68.7	78.9	79.1	67.6	54.8	82.6	74.4	58.5	84.8	72.2
AaD [37]	✓	✗	✗	59.3	79.3	82.1	68.9	79.8	79.5	67.2	57.4	83.1	72.1	58.5	85.4	72.7
AdaCon [38]	✓	✗	✗	47.2	75.1	75.5	60.7	73.3	73.2	60.2	45.2	76.6	65.6	48.3	79.1	65.0
CoWA [39]	✓	✗	✗	56.9	78.4	81.0	69.1	80.0	79.9	67.7	57.2	82.4	72.8	60.5	84.5	72.5
SCLM [40]	✓	✗	✗	58.2	80.3	81.5	69.3	79.0	80.7	69.0	56.8	82.7	74.7	60.6	85.0	73.0
ELR [41]	✓	✗	✗	58.4	78.7	81.5	69.2	79.5	79.3	66.3	58.0	82.6	73.4	59.8	85.1	72.6
PLUE [33]	✓	✗	✗	49.1	73.5	78.2	62.9	73.5	74.5	62.2	48.3	78.6	68.6	51.8	81.5	66.9
TPDS [31]	✓	✗	✗	59.3	80.3	82.1	70.6	79.4	80.9	69.8	56.8	82.1	74.5	61.2	85.3	73.5
C-SFDA [8]	✓	✗	✗	60.3	80.2	82.9	69.3	80.1	78.8	67.3	58.1	83.4	73.6	61.3	86.3	73.5
PSAT-GDA [30]	✓	✗	✓	<u>73.1</u>	88.1	<u>89.2</u>	82.1	88.8	<u>88.9</u>	<u>83.0</u>	<u>72.0</u>	<u>89.6</u>	83.3	<u>73.7</u>	<u>91.3</u>	83.6
LCFD-C-RN [42]	✓	✓	✗	60.1	85.6	86.2	77.2	86.0	86.3	76.6	61.0	86.5	77.5	61.4	86.2	77.6
LCFD-C-B32 [42]	✓	✓	✓	72.3	89.8	89.9	81.1	90.3	89.5	80.1	71.5	89.8	81.8	72.7	90.4	83.3
DIFO-C-RN [5]	✓	✓	✗	62.6	87.5	87.1	79.5	87.9	87.4	78.3	63.4	88.1	80.0	63.7	87.7	79.4
DIFO-C-B32 [5]	✓	✓	✓	70.6	<u>90.6</u>	88.8	<u>82.5</u>	<u>90.6</u>	88.8	80.9	70.1	88.9	<u>83.4</u>	70.5	91.2	83.1
CLIP-RN [24]*	-	✓	✗	51.7	85.0	83.7	69.3	85.0	83.7	69.3	51.7	83.7	69.3	51.7	85.0	72.4
LLaVA-34B [10]*	-	✓	✓	78.3	93.7	89.5	87.0	93.7	89.5	87.0	78.3	89.5	87.0	78.3	93.7	87.2
InstBLIP-XXL [7]*	-	✓	✓	82.0	91.6	88.8	82.2	91.6	88.8	82.2	82.0	88.8	82.2	82.0	91.6	86.2
ShrGPT4V-13B [11]*	-	✓	✓	66.7	85.8	84.8	83.2	85.8	84.8	83.2	66.7	84.8	83.2	66.7	85.8	80.1
RCL (Ours)	✓	✗	✗	82.5	95.3	93.3	89.1	95.3	92.7	89.3	82.4	92.8	89.4	82.1	95.4	90.0

Table 3: Accuracy (%) on the **DomainNet**.

Method	SF	CP	ViT	C→P	C→R	C→S	P→C	P→R	P→S	R→C	R→P	R→S	S→C	S→P	S→R	Avg.
Source	-	✗	✗	42.6	53.7	51.9	52.9	66.7	51.6	49.1	56.8	43.9	60.9	48.6	53.2	52.7
DAPL-RN [1]	✗	✓	✗	72.4	87.6	65.9	72.7	87.6	65.6	73.2	72.4	66.2	73.8	72.9	87.8	74.8
ADCLIP-RN [2]	✗	✓	✗	71.7	88.1	66.0	73.2	86.9	65.2	73.6	73.0	68.4	72.3	74.2	<u>89.3</u>	75.2
SHOT [29]	✓	✗	✗	63.5	78.2	59.5	67.9	81.3	61.7	67.7	67.6	57.8	70.2	64.0	78.0	68.1
NRC [35]	✓	✗	✗	62.6	77.1	58.3	62.9	81.3	60.7	64.7	69.4	58.7	69.4	65.8	78.7	67.5
GKD [36]	✓	✗	✗	61.4	77.4	60.3	69.6	81.4	63.2	68.3	68.4	59.5	71.5	65.2	77.6	68.7
AdaCon [38]	✓	✗	✗	60.8	74.8	55.9	62.2	78.3	58.2	63.1	68.1	55.6	67.1	66.0	75.4	65.4
CoWA [39]	✓	✗	✗	64.6	80.6	60.6	66.2	79.8	60.8	69.0	67.2	60.0	69.0	65.8	79.9	68.6
PLUE [33]	✓	✗	✗	59.8	74.0	56.0	61.6	78.5	57.9	61.6	65.9	53.8	67.5	64.3	76.0	64.7
TPDS [31]	✓	✗	✗	62.9	77.1	59.8	65.6	79.0	61.5	66.4	67.0	58.2	68.6	64.3	75.3	67.1
LCFD-C-RN [42]	✓	✓	✗	75.4	88.2	72.0	75.8	88.3	72.1	76.1	75.6	71.2	77.6	75.9	88.2	78.0
LCFD-C-B32 [42]	✓	✓	✓	77.2	88.0	75.2	78.8	88.2	75.8	79.1	77.8	74.9	79.9	77.4	88.0	80.0
DIFO-C-RN [5]	✓	✓	✗	73.8	<u>89.0</u>	69.4	74.0	<u>88.7</u>	70.1	74.8	74.6	69.6	74.7	74.3	88.0	76.7
DIFO-C-B32 [5]	✓	✓	✓	<u>76.6</u>	87.2	<u>74.9</u>	<u>80.0</u>	87.4	<u>75.6</u>	<u>80.8</u>	<u>77.3</u>	<u>75.5</u>	<u>80.5</u>	<u>76.7</u>	87.3	<u>80.0</u>
LLaVA-34B [10]*	-	✓	✓	84.4	91.0	83.7	85.5	91.0	83.7	85.5	84.4	83.7	85.5	84.4	91.0	86.1
InstBLIP-XXL [7]*	-	✓	✓	82.5	89.0	83.0	86.7	89.0	83.0	86.7	82.5	83.0	86.7	82.5	89.0	85.3
ShrGPT4V-13B [11]*	-	✓	✓	79.7	87.9	79.2	79.9	87.9	79.2	79.9	79.7	79.2	79.9	79.7	87.9	81.7
RCL (Ours)	✓	✗	✗	87.6	92.8	87.9	89.2	92.7	87.8	89.6	87.7	87.6	89.4	87.5	92.7	89.4

4.2 Main results

Our results for Office-Home, DomainNet, and VisDA are presented in Tables 2, 3, and 4, respectively. From top to bottom, we present domain adaptation methods that use source data and CLIP-based techniques, followed by source-free methods without using multimodal or CLIP, and finally, CLIP-based multimodal methods. We also provide zero-shot MLLM/CLIP performance as a reference. RCL consistently achieves state-of-the-art performance on all datasets by showing substantial improvements: **+6.4%** on Office-Home, **+9.4%** on DomainNet, and **+2.9%** on VisDA-C. Notably, the previously best-performing methods, DIFO-C-B32 [5] and DIFO-C-RN [5], utilize a CLIP encoder with ViT-B/32 and a ResNet CLIP backbone, respectively, both leveraging task-specific prompt

learning. In contrast, RCL outperforms these methods using only the source ResNet backbone and guided curriculum training through the integration of MLLM pseudo-labels, RKT, SMKE, and MMR strategies, without relying on prompt learning. Importantly, our self-refinement and curriculum learning processes lead to better performance than the MLLMs themselves, emphasizing the value of our curriculum learning process in learning valuable latent information in the target domain that MLLMs are not capturing. Furthermore, our method using pseudo-label reliability leverages all of the data to train. Unlike prior works, our method utilizes zero-shot MLLM inference capability and hence does not need any customization, prompt learning, or heavy training of multimodal models.

Table 4: Accuracy (%) on the VisDA-C.

Method	SF	CP	ViT	plane	bcyle	bus	car	horse	knife	mcycl	person	plant	sktbrd	train	truck	Avg.
Source	-	X	X	60.4	22.5	44.8	73.4	60.6	3.28	81.3	22.1	62.2	24.8	83.7	4.81	45.3
DAPL-RN [1]	X	✓	X	97.8	83.1	88.8	77.9	97.4	91.5	94.2	79.7	88.6	89.3	92.5	62.0	86.9
PADCLIP-RN [2]	X	✓	X	96.7	88.8	87.0	82.8	97.1	93.0	91.3	83.0	95.5	91.8	91.5	63.0	88.5
ADCLIP-RN [3]	X	✓	X	98.1	83.6	91.2	76.6	98.1	93.4	96.0	81.4	86.4	91.5	92.1	64.2	87.7
SHOT [29]	✓	X	X	95.0	87.4	80.9	57.6	93.9	94.1	79.4	80.4	90.9	89.8	85.8	57.5	82.7
NRC [35]	✓	X	X	96.8	91.3	82.4	62.4	96.2	95.9	86.1	90.7	94.8	94.1	90.4	59.7	85.9
GKD [36]	✓	X	X	95.3	87.6	81.7	58.1	93.9	94.0	80.0	80.0	91.2	91.0	86.9	56.1	83.0
AaD [37]	✓	X	X	97.4	90.5	80.8	76.2	97.3	96.1	89.8	82.9	95.5	93.0	92.0	64.7	88.0
AdaCon [38]	✓	X	X	97.0	84.7	84.0	77.3	96.7	93.8	91.9	84.8	94.3	93.1	94.1	49.7	86.8
CoWA [39]	✓	X	X	96.2	89.7	83.9	73.8	96.4	97.4	89.3	86.8	94.6	92.1	88.7	53.8	86.9
SCLM [40]	✓	X	X	97.1	90.7	85.6	62.0	97.3	94.6	81.8	84.3	93.6	92.8	88.0	55.9	85.3
ELR [41]	✓	X	X	97.1	89.7	82.7	62.0	96.2	97.0	87.6	81.2	93.7	94.1	90.2	58.6	85.8
PLUE [33]	✓	X	X	94.4	91.7	89.0	70.5	96.6	94.9	92.2	88.8	92.9	95.3	91.4	61.6	88.3
TPDS [31]	✓	X	X	97.6	91.5	89.7	83.4	97.5	96.3	92.2	82.4	<u>96.0</u>	94.1	90.9	40.4	87.6
C-SFDA [8]	✓	X	X	97.6	88.8	86.1	72.2	97.2	94.4	92.1	84.7	93.0	90.7	93.1	63.5	87.8
PSAT-GDA [30]	✓	X	✓	97.5	<u>92.4</u>	89.9	72.5	<u>98.2</u>	96.5	89.3	55.6	95.7	98.2	<u>95.3</u>	54.8	86.3
DIFO-C-RN [5]	✓	✓	X	<u>97.7</u>	87.6	90.5	83.6	96.7	95.8	<u>94.8</u>	74.1	92.4	93.8	92.9	65.5	88.8
DIFO-C-B32 [5]	✓	✓	✓	97.5	89.0	<u>90.8</u>	<u>83.5</u>	97.8	97.3	93.2	83.5	95.2	96.8	93.7	<u>65.9</u>	<u>90.3</u>
LLaVA-34B [10]*	-	✓	✓	99.4	97.3	94.8	83.9	98.9	95.8	95.9	80.9	92.7	98.8	97.4	68.9	92.1
InstBLIP-XXL [7]*	-	✓	✓	99.2	89.6	82.0	69.8	97.9	91.0	97.5	84.3	73.6	99.3	96.7	60.0	86.7
ShrGPT4V-13B [11]*	-	✓	✓	99.2	94.7	90.8	87.9	98.3	92.1	97.3	68.0	96.3	95.6	96.8	68.2	90.4
RCL (Ours)	✓	X	X	99.5	96.1	92.6	89.4	99.1	<u>97.1</u>	97.0	<u>85.8</u>	96.6	<u>98.1</u>	97.3	70.0	93.2

4.3 Ablation study

Impact of RCL components. Table 5 presents the results of evaluating the individual components of our method, RCL. When only using RKT, we observe the lowest performance. This outcome is expected, as RKT primarily leverages the most reliable MLLM pseudo-labels to guide learning. However, these labels may not encompass all classes or sufficient diversity (see Figure 9). However, RKT provides the model with adequate supervision in the early stages to begin identifying crucial features. We then observe that applying MMR immediately after RKT results in lower performance compared to applying SMKE. We believe this discrepancy occurs because, although RKT establishes a strong foundation, the model still lacks robustness. Hence, applying SMKE, the model can use less reliable pseudo-labels to increase its knowledge. Finally, there is a consistent improvement in performance when MMR is applied following SMKE, which uses all available data and engages the most unreliable labels in a semi-supervised manner. This approach maximizes the utilization of the model’s learned capabilities, and effectively leverages the entire dataset. Figure 5 visually shows the feature distributions of existing SOTA methods (DIFO) and ours (RCL), emphasising the impact of RKT, SMKE, and MMR techniques in progressively refining the target features.

Table 5: Accuracy (%) of various components of RCL training for select adaptation tasks.

RCL			Office-Home											Avg.	
RKT	SMKE	MMR	A→C	A→P	A→R	C→A	C→P	C→R	P→A	P→C	P→R	R→A	R→C	R→P	
✓	X	X	73.5	89.3	88.2	82.6	89.1	87.9	82.7	73.2	88.2	83.1	73.2	89.4	83.3
✓	X	✓	80.3	93.9	91.9	87.3	94.2	91.8	87.8	80.1	92.2	88.0	80.4	91.9	88.3
✓	✓	X	81.1	95.1	92.7	88.5	95.0	92.3	88.5	80.8	92.4	88.6	80.8	95.3	89.3
✓	✓	✓	82.5	95.3	93.3	89.1	95.3	92.7	89.3	82.4	92.8	89.4	82.1	95.4	90.0

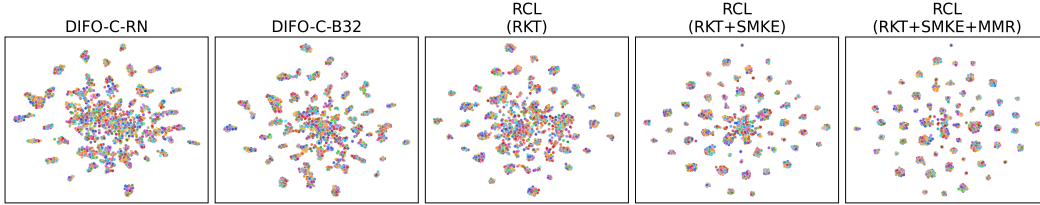


Figure 5: Feature distribution t-SNE visualization comparison on transfer task A→C in Office-Home.

Sensitivity to the capability of MLLMs. As shown in Figure 6, when replacing the best-performing MLLM (LLaVA-34B) with CLIP-RN50, which has a 14.8% lower accuracy on the target task and a 4.9% lower average accuracy when combined with InstructBLIP-XXL and ShareGPT4V-13B, the performance of RCL only decreases by 1.3%. Furthermore, even when using MLLM/CLIP models with an average accuracy of 72.9%, RCL can still maintain an 81.1% accuracy, which is comparable to SOTA methods. This shows that RCL is robust to the choice of MLLMs and highlights its effectiveness in leveraging knowledge from multiple sources and adapting to the target domain. We also studied direct distillation from only one MLLM without RCL. As shown in Figure 7, when the model is learning from one single MLLM, it cannot outperform the MLLM with an upper-bound of MLLM’s zero-shot ability. In contrast, RCL outperforms all the MLLMs it learns from, demonstrating that RCL goes beyond the performance of individual MLLMs by effectively combining their knowledge and adapting it to the target domain through our proposed curriculum learning framework.

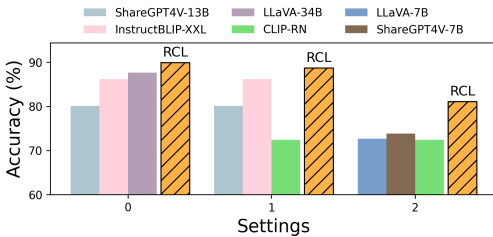


Figure 6: RCL’s sensitivity and robustness against MLLMs with weaker capability.

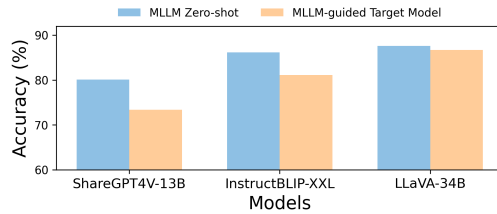


Figure 7: Direct distillation from one MLLM (no RCL) cannot outperform the teacher model.

Knowledge transfer to a smaller backbone. We investigate transferring to a smaller backbone for the scalability of SFDA. As shown in Table 6, RCL can achieve similar results when using ResNet18 compared to ResNet50. It still achieves a +6.4% higher accuracy compared to state-of-the-art methods. With twice the speed (2 GFLOPS vs 4 GFLOPS), RCL effectively exploits the pre-trained knowledge and distills it to a smaller backbone, which is preferable by large-scale inference after training for diverse tasks. This demonstrates RCL’s ability to efficiently leverage the knowledge from MLLMs and adapt it to a lightweight model for the real-world deployment.

Table 6: Impact of Backbone.

Method	BB	Office-Home												Avg.
		A→C	A→P	A→R	C→A	C→P	C→R	P→A	P→C	P→R	R→A	R→C	R→P	
DIFO-C-RN	RN50	62.6	87.5	87.1	79.5	87.9	87.4	78.3	63.4	88.1	80.0	63.3	87.7	79.4
DIFO-C-ViT	RN50	70.6	90.6	88.8	82.5	90.6	88.8	80.9	70.1	88.9	83.4	70.5	91.2	83.1
RCL (Ours)	RN18	81.2	95.3	92.8	88.9	94.9	92.4	88.8	81.7	92.4	89.5	81.6	95.1	89.6
RCL (Ours)	RN50	82.5	95.3	93.3	89.1	95.3	92.7	89.3	82.4	92.8	89.4	82.1	95.4	90.0

The effect of confidence threshold. Figure 8 illustrates the effect of the confidence threshold τ in SMKE. It shows how varying τ values influence model performance by balancing self-correction with MLLM guidance. Higher τ values increase reliance on high-confidence pseudo-labels from the target model, while lower values depend more on MLLM-generated pseudo-labels. The figure

highlights the optimal τ that enhances adaptation performance by effectively leveraging both reliable and less reliable pseudo-labels.

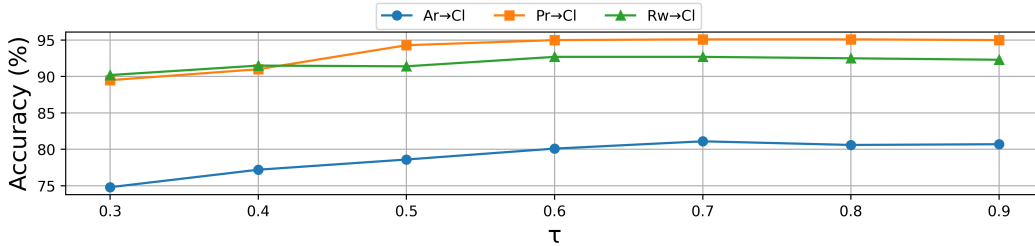


Figure 8: The effect of τ in SMKE.

Pseudo-label reliability with MLLMs Figure 9 demonstrates the distribution of sample reliability across different classes within the Office-Home dataset. We observe that for various classes across domains, there are no or very few samples with $R=1$ (high reliability). This emphasizes the importance of utilizing less reliable data, a fundamental aspect of our approach, which is integrated into our SMKE and MMR techniques. To highlight our point, if we observe Table 5, it is evident that using only $R=1$ data (applying only RKT) results in notably lower accuracies for the Clipart domain (while adaptations to other domains achieve over 80%, Clipart is lowest at 73.3%). As Figure 9 indicates, the Clipart domain has a higher proportion of pseudo-labels where $0 < R < 1$. By employing SMKE and MMR, we manage to enhance performance in adapting to the Clipart domain by +9% (to 82.3%).

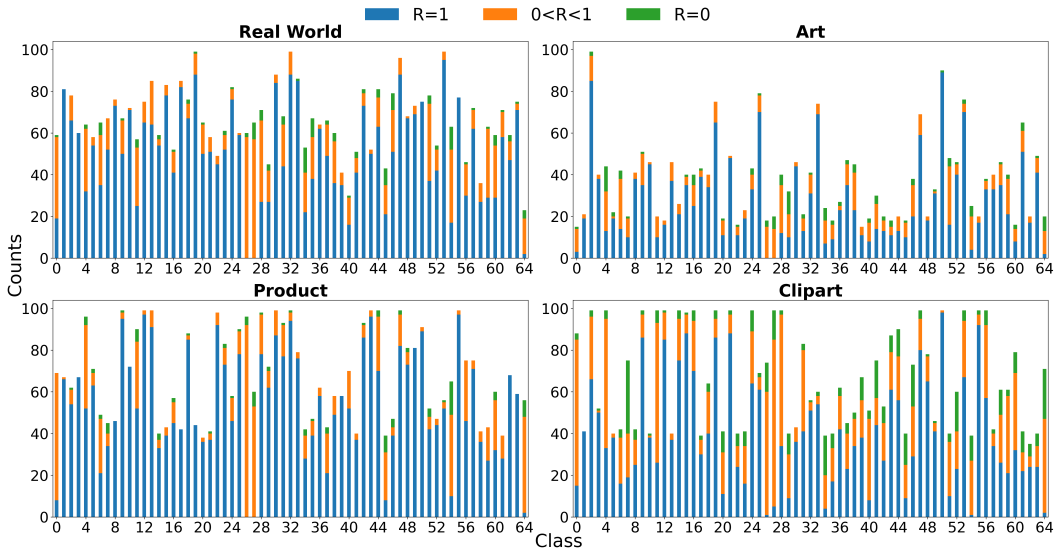


Figure 9: Per-class counts of MLLM pseudolabels on Office-Home.

Implementation of Pseudo-labeling with MLLMs For the STS calculations, we utilize all-MiniLM-L6-v2 [43] to generate vector representations of both the outputs from the MLLMs and the text options. To facilitate pseudo-labeling, we design specific prompt templates for different MLLMs:

For LLaVA models: "What is the closest name from this list to describe the object in the image? Return the name only. <class names>"

For ShareGPT4V models: "Question: What is the closest name from this list to describe the object in the image? List: <class names> Return the closest name from the list only. Use *exact* names from the list only. Answer:"

For InstructBLIP models: "Question: What is the closest name from this list to describe the object in the image? <class names>. Use the closest name from the list only. Pick the answer from the list only. Answer:"

5 Discussion

In this work, we propose a novel method for adapting foundational knowledge of pre-trained Multi-Modal Large Language Models (MLLMs) to significantly enhance the capability of models in Source-Free Domain Adaptation (SFDA). Our novel approach leverages MLLMs’ pre-trained knowledge through a curriculum learning strategy that uniquely integrates insights from diverse MLLMs. This strategy goes beyond mere utilization of existing knowledge; it actively adapts and refines it through a reliability-based knowledge transfer mechanism and a dynamic, self-correcting learning process. Additionally, our integration of a Multi-hot Masking Refinement technique in a semi-supervised manner within the curriculum learning framework facilitates precise, targeted adaptation of the model. Our method achieves state-of-the-art results across standard benchmarks and even surpasses the baseline performance of MLLMs.

Limitation. Inherent generalizability and biases from pre-trained MLLMs may constrain our model, although we attempted to alleviate these with a consensus approach utilizing multiple MLLMs.

References

- [1] Chunjiang Ge, Rui Huang, Mixue Xie, Zihang Lai, Shiji Song, Shuang Li, and Gao Huang. Domain adaptation via prompt learning. *IEEE Transactions on Neural Networks and Learning Systems*, 2023.
- [2] Zhengfeng Lai, Noranart Vesdapunt, Ning Zhou, Jun Wu, Cong Phuoc Huynh, Xuelu Li, Kah Kuen Fu, and Chen-Nee Chuah. Padclip: Pseudo-labeling with adaptive debiasing in clip for unsupervised domain adaptation. In *ICCV*, 2023.
- [3] Mainak Singha, Harsh Pal, Ankit Jha, and Biplab Banerjee. Ad-clip: Adapting domains in prompt space using clip. In *ICCV Workshop*, 2023.
- [4] Jian Liang, Dapeng Hu, and Jiashi Feng. Shot: Source hypothesis transfer for unsupervised domain adaptation. In *Conference on Computer Vision and Pattern Recognition (CVPR)*, 2021.
- [5] Song Tang, Wenxin Su, Mao Ye, and Xiatian Zhu. Source-free domain adaptation with frozen multimodal foundation model. In *Conference on Computer Vision and Pattern Recognition (CVPR)*, 2024.
- [6] Haotian Liu, Chunyuan Li, Yuheng Li, and Yong Jae Lee. Improved baselines with visual instruction tuning. In *NeurIPS 2023 Workshop on Instruction Tuning and Instruction Following*, 2023.
- [7] Wenliang Dai, Junnan Li, Dongxu Li, Anthony Meng Huat Tiong, Junqi Zhao, Weisheng Wang, Boyang Li, Pascale N Fung, and Steven Hoi. Instructblip: Towards general-purpose vision-language models with instruction tuning. *Advances in Neural Information Processing Systems*, 36, 2024.
- [8] Nazmul Karim, Niluthpol Chowdhury Mithun, Abhinav Rajvanshi, Han-pang Chiu, Supun Samarasekera, and Nazanin Rahnavard. C-sfda: A curriculum learning aided self-training framework for efficient source free domain adaptation. In *Proceedings of the IEEE/CVF Conference on Computer Vision and Pattern Recognition*, pages 24120–24131, 2023.
- [9] Tsung-Yi Lin, Michael Maire, Serge Belongie, James Hays, Pietro Perona, Deva Ramanan, Piotr Dollár, and C Lawrence Zitnick. Microsoft coco: Common objects in context. In *Computer Vision—ECCV 2014: 13th European Conference, Zurich, Switzerland, September 6-12, 2014, Proceedings, Part V 13*, pages 740–755. Springer, 2014.
- [10] Haotian Liu, Chunyuan Li, Qingyang Wu, and Yong Jae Lee. Visual instruction tuning. In *NeurIPS*, 2023.
- [11] Lin Chen, Jisong Li, Xiaoyi Dong, Pan Zhang, Conghui He, Jiaqi Wang, Feng Zhao, and Dahua Lin. Sharegpt4v: Improving large multi-modal models with better captions. *arXiv preprint arXiv:2311.12793*, 2023.

- [12] Liang Chen, Haozhe Zhao, Tianyu Liu, Shuai Bai, Junyang Lin, Chang Zhou, and Baobao Chang. An image is worth 1/2 tokens after layer 2: Plug-and-play inference acceleration for large vision-language models. *arXiv preprint arXiv:2403.06764*, 2024.
- [13] Kate Saenko, Brian Kulis, Mario Fritz, and Trevor Darrell. Adapting visual category models to new domains. In *Computer Vision—ECCV 2010: 11th European Conference on Computer Vision, Heraklion, Crete, Greece, September 5–11, 2010, Proceedings, Part IV 11*, pages 213–226. Springer, 2010.
- [14] Xingchao Peng, Qinxun Bai, Xide Xia, Zijun Huang, Kate Saenko, and Bo Wang. Moment matching for multi-source domain adaptation. In *Proceedings of the IEEE/CVF international conference on computer vision*, pages 1406–1415, 2019.
- [15] Xingchao Peng, Ben Usman, Neela Kaushik, Judy Hoffman, Dequan Wang, and Kate Saenko. Visda: The visual domain adaptation challenge. *arXiv preprint arXiv:1710.06924*, 2017.
- [16] Jingjing Jiang, Ke Chen, and Hao Yang. Neighborhood reconstructed clustering for source-free domain adaptation. In *Conference on Computer Vision and Pattern Recognition (CVPR)*, 2022.
- [17] Song Tang, Yan Yang, Zhiyuan Ma, Norman Hendrich, Fanyu Zeng, Shuzhi Sam Ge, Changshui Zhang, and Jianwei Zhang. Nearest neighborhood-based deep clustering for source data-absent unsupervised domain adaptation. *arXiv:2107.12585*, 2021.
- [18] Song Tang, Yan Zou, Zihao Song, Jianzhi Lyu, Lijuan Chen, Mao Ye, Shouming Zhong, and Jianwei Zhang. Semantic consistency learning on manifold for source data-free unsupervised domain adaptation. *Neural Networks*, 152:467–478, 2022.
- [19] Sanqing Qu, Guang Chen, Jing Zhang, Zhijun Li, Wei He, and Dacheng Tao. Bmd: A general class-balanced multicentric dynamic prototype strategy for source-free domain adaptation. In *European conference on computer vision*, pages 165–182. Springer, 2022.
- [20] Weijie Chen, LuoJun Lin, Shicai Yang, Di Xie, Shiliang Pu, and Yueting Zhuang. Self-supervised noisy label learning for source-free unsupervised domain adaptation. In *2022 IEEE/RSJ International Conference on Intelligent Robots and Systems (IROS)*, pages 10185–10192. IEEE, 2022.
- [21] Mattia Litrico, Alessio Del Bue, and Pietro Morerio. Guiding pseudo-labels with uncertainty estimation for source-free unsupervised domain adaptation. In *Proceedings of the IEEE/CVF Conference on Computer Vision and Pattern Recognition*, pages 7640–7650, 2023.
- [22] Shiqi Yang, Yaxing Wang, Joost Van De Weijer, Luis Herranz, and Shangling Jui. Generalized source-free domain adaptation. In *Proceedings of the IEEE/CVF international conference on computer vision*, pages 8978–8987, 2021.
- [23] Ning Ding, Yixing Xu, Yehui Tang, Chao Xu, Yunhe Wang, and Dacheng Tao. Source-free domain adaptation via distribution estimation. In *Proceedings of the IEEE/CVF conference on computer vision and pattern recognition*, pages 7212–7222, 2022.
- [24] Alec Radford, Jong Wook Kim, Chris Hallacy, Aditya Ramesh, Gabriel Goh, Sandhini Agarwal, Girish Sastry, Amanda Askell, Pamela Mishkin, Jack Clark, et al. Learning transferable visual models from natural language supervision. *arXiv preprint arXiv:2103.00020*, 2021.
- [25] Chao Jia, Yinfei Yang, Ye Xia, Yi-Ting Chen, Zarana Parekh, Hieu Pham, Quoc V Le, Yun-Hsuan Sung, Zhen Li, and Tom Duerig. Align: Towards bridging alignment for large-scale multi-modal understanding. In *International Conference on Machine Learning (ICML)*, 2021.
- [26] Zhengfeng Lai, Haoping Bai, Haotian Zhang, Xianzhi Du, Jiulong Shan, Yinfei Yang, Chen-Nee Chuah, and Meng Cao. Empowering unsupervised domain adaptation with large-scale pre-trained vision-language models. In *Proceedings of the IEEE/CVF Winter Conference on Applications of Computer Vision*, pages 2691–2701, 2024.
- [27] Cairong Zhao, Yubin Wang, Xinyang Jiang, Yifei Shen, Kaitao Song, Dongsheng Li, and Duoqian Miao. Learning domain invariant prompt for vision-language models. *IEEE Transactions on Image Processing*, 2024.

- [28] Thomas Westfechtel, Dexuan Zhang, and Tatsuya Harada. Combining inherent knowledge of vision-language models with unsupervised domain adaptation through self-knowledge distillation. *arXiv preprint arXiv:2312.04066*, 2023.
- [29] Jian Liang, Dapeng Hu, and Jiashi Feng. Do we really need to access the source data? source hypothesis transfer for unsupervised domain adaptation. In *ICML*, 2020.
- [30] Song Tang, Yuji Shi, Zihao Song, Mao Ye, Changshui Zhang, and Jianwei Zhang. Progressive source-aware transformer for generalized source-free domain adaptation. *IEEE Transactions on Multimedia*, 2023.
- [31] Song Tang, An Chang, Fabian Zhang, Xiatian Zhu, Mao Ye, and Changshui Zhang. Source-free domain adaptation via target prediction distribution searching. *International Journal of Computer Vision*, pages 1–19, 2023.
- [32] Kaiming He, Xiangyu Zhang, Shaoqing Ren, and Jian Sun. Deep residual learning for image recognition. In *Proceedings of the IEEE conference on computer vision and pattern recognition*, pages 770–778, 2016.
- [33] Mattia Litrico, Alessio Del Bue, and Pietro Morerio. Guiding pseudo-labels with uncertainty estimation for source-free unsupervised domain adaptation. In *CVPR*, 2023.
- [34] Diederik P. Kingma and Jimmy Ba. Adam: A method for stochastic optimization. In *International Conference on Learning Representations*, 2015.
- [35] Shiqi Yang, Joost van de Weijer, Luis Herranz, Shangling Jui, et al. Exploiting the intrinsic neighborhood structure for source-free domain adaptation. In *NeurIPS*, 2021.
- [36] S Tang, Yuji Shi, Zhiyuan Ma, Jian Li, Jianzhi Lyu, Qingdu Li, and Jianwei Zhang. Model adaptation through hypothesis transfer with gradual knowledge distillation. In *IROS*, 2021.
- [37] Shiqi Yang, Yaxing Wang, Kai Wang, Shangling Jui, et al. Attracting and dispersing: A simple approach for source-free domain adaptation. In *NeurIPS*, 2022.
- [38] Dian Chen, Dequan Wang, Trevor Darrell, and Sayna Ebrahimi. Contrastive test-time adaptation. In *CVPR*, 2022.
- [39] Jonghyun Lee, Dahuin Jung, Junho Yim, and Sungroh Yoon. Confidence score for source-free unsupervised domain adaptation. In *ICML*, 2022.
- [40] Song Tang, Yan Zou, Zihao Song, Jianzhi Lyu, Lijuan Chen, Mao Ye, Shouming Zhong, and Jianwei Zhang. Semantic consistency learning on manifold for source data-free unsupervised domain adaptation. *Neural Networks*, 152, 2022.
- [41] Li Yi, Gezheng Xu, Pengcheng Xu, Jiaqi Li, Ruizhi Pu, Charles Ling, A Ian McLeod, and Boyu Wang. When source-free domain adaptation meets learning with noisy labels. In *ICLR*, 2023.
- [42] Song Tang, Wenxin Su, Mao Ye, Jianwei Zhang, and Xiatian Zhu. Unified source-free domain adaptation. *arXiv preprint arXiv:2403.07601*, 2024.
- [43] Nils Reimers and Iryna Gurevych. Making monolingual sentence embeddings multilingual using knowledge distillation. In *Proceedings of the 2020 Conference on Empirical Methods in Natural Language Processing*. Association for Computational Linguistics, 11 2020. URL <https://arxiv.org/abs/2004.09813>.